Fault permeability from stochastic modeling of clay smears

Article *in* Geology · December 2022

DOI: 10.1130/G50739.1

3 authors, including:

Lluís Saló-Salgado
Harvard University
11 PUBLICATIONS **56** CITATIONS

SEE PROFILE

GEOLOGY | THE GEOLOGICAL SOCIETY OF AMERICA®

https://doi.org/10.1130/G50739.1

Manuscript received 14 July 2022
Revised manuscript received 7 September 2022
Manuscript accepted 9 September 2022

Published online 5 December 2022

Fault permeability from stochastic modeling of clay smears

Lluís Saló-Salgado[1,2], J. Steven Davis[3]* and Ruben Juanes[1,2]

[1]Department of Civil and Environmental Engineering, Massachusetts Institute of Technology, 77 Massachusetts Avenue, Cambridge, Massachusetts 02139, USA

[2]Earth Resources Laboratory, Department of Earth, Atmospheric and Planetary Sciences, Massachusetts Institute of Technology, 77 Massachusetts Avenue, Cambridge, Massachusetts 02139, USA

[3]ExxonMobil Upstream Integrated Solutions Company, 22777 Springwoods Village Parkway, Spring, Texas 77389, USA

ABSTRACT

In normally consolidated, shallow (depth <~3 km) siliciclastic sequences, faults develop clay smears. Existing models include the dependence of permeability on the clay fraction, but improved predictions of fault permeability should account for uncertainty and anisotropy. We introduce PREDICT, a methodology that computes probability distributions for the directional components (dip-normal, strike-parallel, and dip-parallel) of the fault permeability tensor from statistical samples for a set of geological variables. These variables, which include geometrical, compositional, and mechanical properties, allow multiple discretizations of the fault core to be populated with sand and clay smears, which can be used to upscale the permeability to a coarser scale (e.g., suitable for reservoir modeling). We validated our implementation with experimental data and applied PREDICT to several stratigraphic sequences. We show that fault permeability is controlled by the clay smear configuration and, crucially, that it typically exhibits multimodal probability distributions due to the existence of holes. The latter is a unique feature of our algorithm, which can be used to build fault permeability scenarios to manage and mitigate risk in subsurface applications.

INTRODUCTION

As observed by Weber et al. (1978) and Lehner and Pilaar (1997), faults in normally consolidated, shallow (depth <~3 km) sand-clay sequences develop ductile clay smears (see the comprehensive review by Vrolijk et al. [2016]). The influence of clay has been recognized in pioneering models of fault permeability, which were derived from laboratory measurements (Manzocchi et al., 1999; Sperrevik et al., 2002). These models depend on an estimate of the fault clay fraction, which is included through a proxy such as the shale gouge ratio (SGR; Yielding et al., 1997). Subsequent algorithms and models founded on a similar premise have been developed (Jolley et al., 2007; Myers et al., 2014), but they require extensive local data sets. Key shortcomings of this type of model are: scale-independent, averaged upscaling of lithological diversity, which contrasts with the strongly heterogeneous materials in shallow faults (Rawling et al., 2001; Childs et al., 2007; Vrolijk et al., 2016); limited insight on the geologic elements or properties controlling permeability; and the computation of cross-fault permeability only.

To increase generality and better represent outcrop observations, Tveranger et al. (2005) developed the fault facies concept, and Bense and Person (2006) presented an algorithm that includes permeability anisotropy due to vertical layering in the fault zone. Childs et al. (2007) described a probabilistic shale smear predictor; they computed the average smear gap length between a given smearing layer at each side of the fault to calculate the permeability perpendicular to the fault via arithmetic averaging. Grant (2020) focused on fault core sealing and developed a stochastic, facies-based fault permeability algorithm. In the Grant (2020) algorithm, the proportions of different fault rocks and number of material layers in the core are defined by the user; the output permeability, perpendicular to the fault, is computed via harmonic averaging.

The algorithms outlined above are difficult to generalize because a quantitative description of the controls on fault material distribution is lacking, representing a key area to improve fluid-flow predictions in smear-dominated faults (Vrolijk et al., 2016). In addition, previous algorithms do not quantify uncertainty or anisotropy in the directional components (dip-normal, k_{xx}; strike-parallel, k_{yy}; and dip-parallel, k_{zz}) of the fault permeability tensor, which arises from material heterogeneity. This is required to manage and mitigate risk in subsurface applications like geological CO_2 storage (GCS), where flows along faults can be critical (IEAGHG, 2016).

To bridge this gap, we developed PREDICT, a methodology to quantify fault permeability in normally consolidated (NC), shallow (<~3 km) siliciclastic sequences. For example, these conditions are found in Cenozoic sediments in passive margins, and they are relevant for large-scale GCS projects (Ringrose and Meckel, 2019).

STOCHASTIC COMPUTATION OF FAULT PERMEABILITY

PREDICT (the full algorithm description is given in the Supplemental Material[1] and the code is available at https://github.com/lsalo/predict/) computes the directional components of the fault permeability tensor in an upscaling (coarse) grid defined by the user; flexible upscaling is useful to assign fault permeability in subsequent flow simulations. The computation is performed in a given throw window, in which PREDICT represents the fault core (Fig. 1). Consistent with the offset of clay layers across a finite-thickness shear zone, smears are placed at an angle >0 to the fault plane (e.g., Lindsay et al., 1993, their figure 3). Constant throw along strike is assumed. A summary of PREDICT follows.

*Current address: Stanford Center for Carbon Storage, Stanford University, Palo Alto, California 94305, USA

[1]Supplemental Material. Detailed description of the PREDICT methodology. Please visit https://doi.org/10.1130/GEOL.S.21397161 to access the supplemental material and contact editing@geosociety.org with any questions.

CITATION: Saló-Salgado, L., Davis, J.S., and Juanes, R., 2023, Fault permeability from stochastic modeling of clay smears: Geology, v. XX, p. , https://doi.org/10.1130/G50739.1

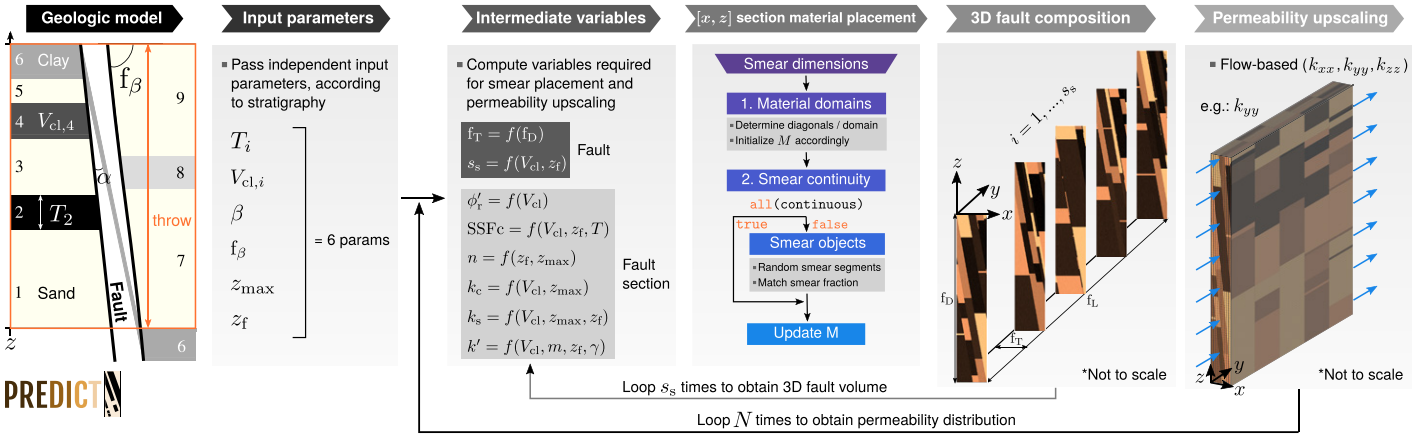

Figure 1. PREDICT workflow (left to right). Stratigraphic section is described by input parameters, which PREDICT uses to compute ranges and probability distributions for intermediate variables. Each three-dimensional (3-D) fault realization is obtained by generating n = s_s fault sections with constant thickness and arranging them along strike. For each fault section, residual friction angle (ϕ'_r), critical shale smear factor (SSFc), porosity (*n*), permeability (*k*), and permeability anisotropy ratio (*k′*) are sampled and used to place fault materials and assign their properties. Subscript "c" refers to clay smear, and "s" refers to sand smear. Permeability is upscaled using 3-D fault volume. See the main text for notation and the Supplemental Material (see footnote 1) for details.

The algorithm requires a set of input parameters that describe the faulted stratigraphy: the layer thickness (T), clay volume fraction (V_{cl}), and dip angle (β), plus the fault dip (f_β), maximum burial depth (z_{max}), and faulting depth (z_f). By combining these inputs as described in S1.2 in the Supplemental Material, PREDICT generates marginal probability distributions (P_x) for another set of numerical quantities: fault thickness (f_T), residual friction angle (ϕ'_r), critical shale smear factor (SSFc) (Færseth, 2006; Childs et al., 2007), porosity (n), permeability (k), permeability anisotropy ratio (k'), and a parameter describing along-strike smear segmentation (s_s). The P_x are used to sample each intermediate variable accounting for dependency, and to populate the fault with clay smears ($V_{cl} \geq 0.4$) and sand smears ($V_{cl} < 0.4$), according to S1.2 and S1.3 in the Supplemental Material (also see Fig. 1).

To populate the fault, PREDICT first generates a set of strike-perpendicular fault sections (FSs), each discretized with 10^4 cells (S1.4 in the Supplemental Material). Each FS is generated independently and is first subdivided into different domains according to the contributed materials and their thickness. The clay smear thicknesses are computed via Egholm et al.'s equation 5 (2008), which is valid for failure of granular materials with varying friction (see S1.3 in the Supplemental Material), while sand smears fill the remaining f_T. Next, downdip smear continuity is assessed, and object-based simulation is used to place the discontinuous smears in the corresponding domains. After assigning fault materials and their properties to each FS, a three-dimensional (3-D) fault volume is obtained by arranging them along-strike (fine grid). The number of unique FSs in a given 3-D realization is equal to s_s. The 3-D volume has dimensions $f_T \times f_D \times f_L$, where f_D is the fault displacement, and f_L is the length (along-strike), which is set equal to f_D.

Finally, the permeability for the studied throw window is computed in the coarse grid by flow-based upscaling of the fine grid permeability using the MATLAB Reservoir Simulation Toolbox (MRST; Lie, 2019). Multiple realizations of this process result in probability distributions for k_{xx}, k_{yy}, and k_{zz} (see Fig. 1; see the Supplemental Material).

RESULTS AND DISCUSSION

Validation with Experimental Fault-Scale Permeability

We validated our implementation by comparing PREDICT's k_{xx} values to experimental cross-fault permeabilities estimated from flux measurements by Kettermann et al. (2017, their figure 14). Kettermann et al. (2017) presented a set of experiments in a water-saturated sandbox, where sediment faulting was driven by a rigid basement fault, and flow across the sheared clay was induced by lowering the hydraulic head in the bottom reservoir (Fig. 2A). They also presented smear/hole maps (Fig. 2B), which we used to define s_s (Fig. 1; S1.2 in the Supplemental Material). A view of the discontinuous clay smear in PREDICT is shown for one realization (single clay layer) in Figure 2C. The permeability comparison is shown in Figure 2D, where we used a coarse grid with a single cell to obtain our bulk fault permeability. It is apparent that most of PREDICT's probability distribution matches the range defined by the experimentally derived permeabilities (calculation details are given in S3 in the Supplemental Material).

Clay Smear Modeling Leads to Multimodal Fault Permeability Distributions

The effect of increasing the average section clay fraction ($\overline{V_{cl}}$) is illustrated in Figure 3, where multimodal or wider distributions arise when some material configurations lead to unobstructed sand pathways, and others do not (Figs. 3B and 3C). The presence of holes in 3-D clay smears is consistent with previous observations (e.g., Noorsalehi-Garakani et al., 2013). Overall, we found that the main factor determining whether most of the probability is at lower or higher permeability is the frequency of continuous sand pathways (cf. Fig. S17). This frequency is inversely related to the stratigraphic clay fraction, which agrees with previous stochastic models of clay smear (Childs et al., 2007; Yielding, 2012; Grant, 2020) and field evidence (Bense et al., 2013; Vrolijk et al., 2016; and references therein).

Stratigraphic Controls on Fault Permeability

Next, we modeled sequences with the same $\overline{V_{cl}}$ but different layering and burial history. We considered three intervals with $\overline{V_{cl}} = 0.3$, inspired by the Lower Miocene section offshore Texas (Treviño and Meckel, 2017) (Fig. 4A), the Statfjord Formation in the North Sea (Myers et al., 2007) (Fig. 4B), and the Mount Messenger Formation in New Zealand (Childs et al., 2007) (Fig. 4C).

As the clay layer thickness decreased (Figs. 4A–4C), we observed (1) a decrease in the average fault clay fraction (f_{Vcl}), which typically led to higher permeability; and (2) a notable increase in k_{yy} and k_{zz} because of thinner smears. Hence, in agreement with long-standing observations (Weber et al., 1978; Lindsay et al., 1993), the macroscale fault permeability is primarily dependent on the derived smear configurations. This demonstrates the importance of accounting for material heterogeneity.

Fault Clay Fraction and Permeability

Because all three sections in Figure 4 had equal $\overline{V_{cl}}$ and were relatively shallow, the

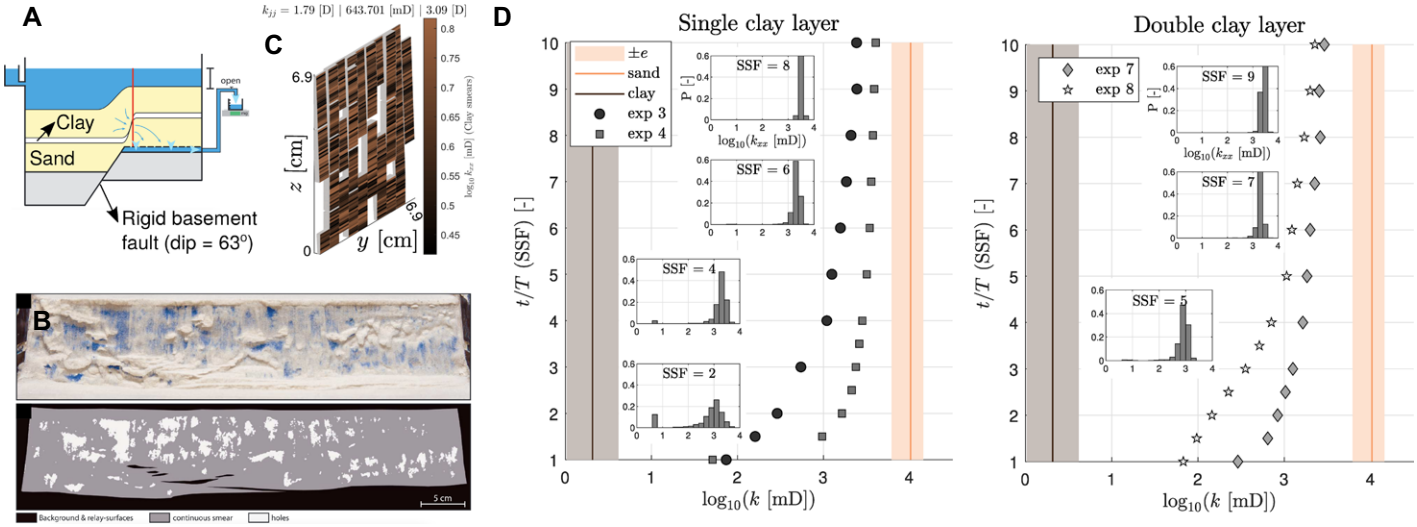

Figure 2. Validation with experimental data from Kettermann et al. (2017). (A) Experimental diagram. (B) Frontal view of excavated fault surface showing discontinuous smear (top) and smear hole mapping (bottom). Both A and B are from Kettermann et al. (2017). (C) PREDICT realization for shale smear factor (SSF) = 6, showing segmented clay smear. Fault dip was set to 60°. (D) Main plots show experimental cross-fault permeabilities (markers) and end-member permeabilities (vertical lines), computed from data in Kettermann et al. (2017) (see section S3 in the Supplemental Material [see footnote 1]). Inset plots show PREDICT's predictions for several SSF values.

permeability calculation according to Sperrevik et al. (2002) (using the SGR) yielded very similar values. This contrasts with PREDICT's output, which showed diminishing f_{Vcl} and different permeability distributions. Our results agree with results by Childs et al. (2007), who showed that their smear-based permeability is lower than the SGR-based permeability where only a few beds are displaced, but they are likely closer as the shale layer thicknesses decrease (cf. Fig. 4).

In Figure 4A, estimated values from Lu et al. (2017) for Miocene mudstone cores from the Gulf of Mexico fall above PREDICT's main mode, which seems to be compatible with their lower V_{cl}. Zheng and Espinoza (2021) reported 10^{-5}–10^{-4} mD for synthetic mixtures of Frio sand and Anahuac shale at 20 MPa effective stress, which is very close to our main mode. Faults in the Mount Messenger Formation were studied by Childs et al. (2007), who reported ranges similar to PREDICT's output (Fig. 4C).

Fault Permeability Uncertainty and Anisotropy

For a given stratigraphy, our analysis showed that multiple smear configurations (and upscaled permeability values) are possible. This reflects (1) the fact that knowledge of the subsurface is insufficient to model faults deterministically (Lunn et al., 2008; Bense et al., 2013; IEAGHG, 2016; Vrolijk et al., 2016), and (2) PREDICT's quantification of this uncertainty.

In PREDICT, permeability anisotropy of fault materials is typically within one order of magnitude. Higher anisotropy, as observed in some realizations in Figures 3 and 4, is the result of material arrangement in the fault. This agrees with previous studies, which show that the maximum anisotropy of sheared clay-rich material

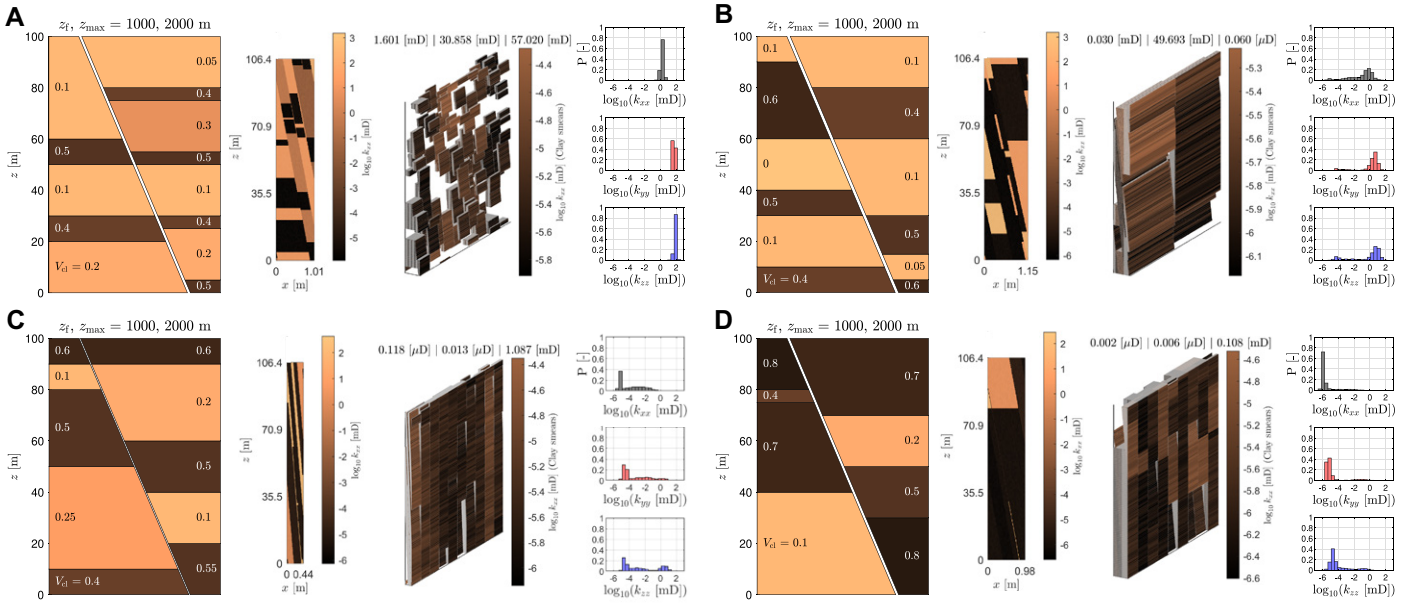

Figure 3. Effect of increasing section average clay fraction ($\overline{V_{cl}}$). Each panel depicts: faulted stratigraphic interval (left); example fault material realization (center), showing frontal (*x*, *z*) cross section on left and clay smear distribution on right (upscaled permeability result shown at the top); and probability (P) distributions of fault permeability using using single cell for upscaling (right). Throw is 100 m in all four cases, and stratigraphy is colored by V_{cl}. (A) $\overline{V_{cl}}$ = 0.21. (B) $\overline{V_{cl}}$ = 0.27. (C) $\overline{V_{cl}}$ = 0.36. (D) $\overline{V_{cl}}$ = 0.53.

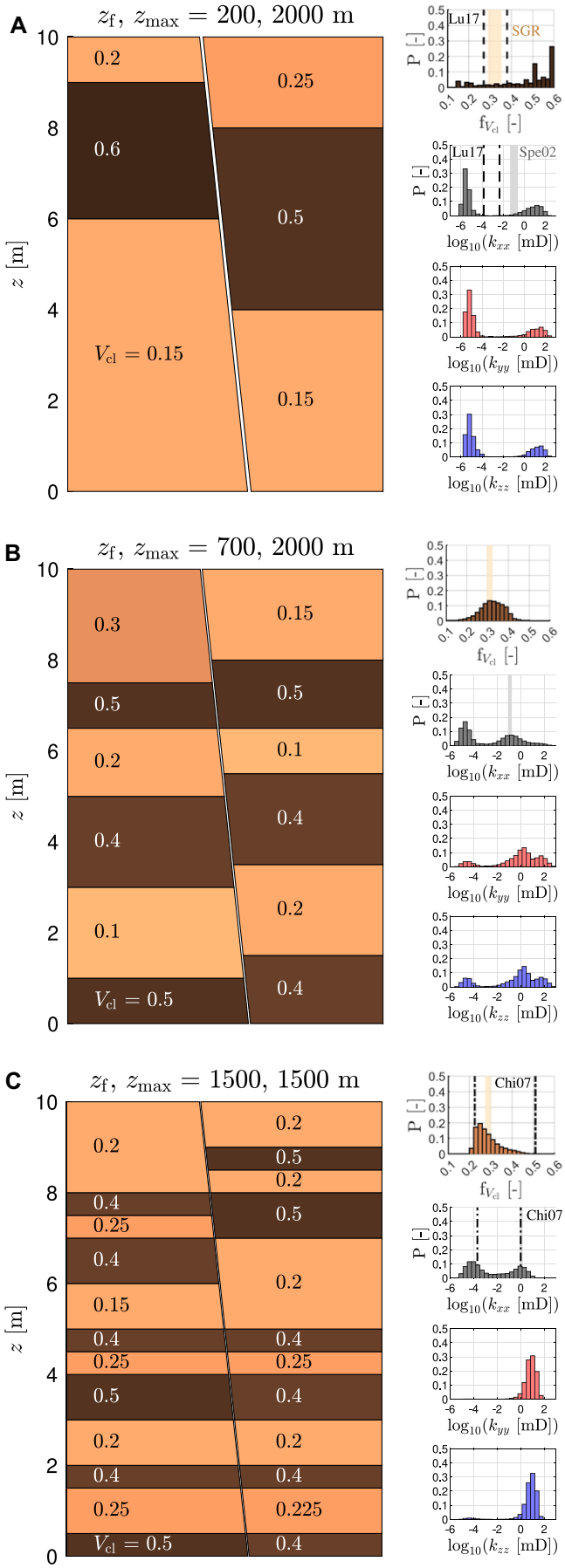

Figure 4. Fault permeability for three sequences with average clay fraction (V_{cl}) = 0.3 and throw = 10 m. Fault thickness in each stratigraphic section is from arbitrary realization. At right: Upscaled probability (P) distributions of average fault clay fraction (fV_{cl}) and fault permeability. Upscaling grid with 2 × 10 × 10 equal cells (*x*, *y*, *z*) was used to make results comparable (in scale) to reported measurements, and all upscaled cell values were collapsed into single distributions. Shale gouge ratio (SGR; orange fill) and resulting permeability range (gray fill) from Sperrevik et al. (2002; Spe02) is also shown. Ranges obtained by Lu et al. (2017; Lu17) and Childs et al. (2007; Chi07) (within 20%–60% phyllosilicate) are plotted with dashed and dash-dotted lines, respectively.

is typically ~10 (Dewhurst et al., 1996; Daigle and Dugan, 2011).

APPLICATION TO FAULT PERMEABILITY MODELING IN REAL SETTINGS

PREDICT models the fault as a shear zone and ignores the occurrence of other smearing mechanisms such as abrasion (Lindsay et al., 1993) and injection (Lehner and Pilaar, 1997). Shear-dominated smear formation is supported by observations in shallow siliciclastic sequences, where the clay layers are dragged into the fault (Weber et al., 1978; Kettermann et al., 2016). Recently, Vrolijk et al. (2016, their figure 27) proposed a framework to characterize the smearing processes, which suggests that our algorithm is most applicable to sequences in which the clay, compared to the sand, is weaker to similarly strong. Considering typical cohesion and friction angles, this is expected in most shallow sequences at hydrostatic pressure and depths below a few tens of meters.

Each 3-D fault core realization was obtained by concatenating serial, equal-length two-dimensional (2-D) sections along-strike, which led to all clay smears being truncated at the same along-strike coordinates (Fig. 1). Additionally, each 3-D fault core realization had a constant thickness. While these geometric choices are a simplification of reality (Lunn et al., 2008; Kettermann et al., 2016; Sosio de Rosa et al., 2018), PREDICT balances this by considering thousands of realizations; in each realization, both fault thickness and the number of concatenated sections change. Clay smears are modeled as tabular bodies, which is a reasonable approximation (Çiftçi et al., 2013; Kettermann et al., 2016, 2017).

Along-strike throw variations cannot be explicitly accounted for, but the algorithm can be quickly run multiple times with varying inputs (e.g., fault displacement). PREDICT has matched experimental bulk fault permeabilities (Fig. 2) and is consistent with local measurements (Fig. 4). PREDICT's quantification of uncertainty and permeability anisotropy unlocks the ability to quantify, manage, and communicate hazards associated with subsurface technologies such as GCS (cf. Bjørnarå et al., 2021; Snippe et al., 2022), natural gas storage, and nuclear waste disposal.

CONCLUSIONS

PREDICT includes a description of smearing in granular materials that is consistent with observations in shallow (depth <~3 km) siliciclastic sequences and incorporates uncertainty in the physical quantities controlling the fault and material dimensions and their properties. The output probability distributions, which characterize the directional components of the fault permeability tensor (dip-normal, strike-parallel, and dip-

parallel) in a coarse grid defined by the user, can be multimodal. Our algorithm provides (1) a parameter-based link among the stratigraphy, the heterogeneous fault core materials, and the macroscale permeability; and (2) the likelihood of different fault permeability scenarios, which is required to assess hazard in subsurface technologies.

ACKNOWLEDGMENTS

This work was funded by ExxonMobil, and we greatly benefited from productive discussions with the team involved. L. Saló-Salgado thanks The MathWorks, Inc., and the Massachusetts Institute of Technology School of Engineering for funding through a 2020–2021 MathWorks Engineering Fellowship. We are grateful to Youssef Marzouk and Ehsan Haghighat for helpful comments on multivariate statistical modeling and to Olav Møyner for outstanding assistance with MRST. Thorough reviews by Graham Yielding and Janos Urai are gratefully acknowledged.

REFERENCES CITED

Bense, V.F., and Person, M., 2006, Faults as conduit-barrier systems to fluid flow in siliciclastic sedimentary aquifers: Water Resources Research, v. 42, W05421, https://doi.org/10.1029/2005WR004480.

Bense, V.F., Gleeson, T., Loveless, S.E., Bour, O., and Scibek, J., 2013, Fault zone hydrogeology: Earth-Science Reviews, v. 127, p. 171–192, https://doi.org/10.1016/j.earscirev.2013.09.008.

Bjørnarå, T.I., Haines, E.M., and Skurtveit, E., 2021, Upscaled geocellular flow model of potential across- and along-fault leakage using shale gouge ratio, *in* Proceedings of the 11th Trondheim Conference on CO_2 Capture, Transport and Storage: Trondheim, Norway, Norwegian CCS Research Centre, p. 366–373, https://sintef.brage.unit.no/sintef-xmlui/handle/11250/2786524.

Childs, C., Walsh, J.J., Manzocchi, T., Strand, J., Nicol, A., Tomasso, M., Schöpfer, M.P., and Aplin, A.C., 2007, Definition of a fault permeability predictor from outcrop studies of a faulted turbidite sequence, Taranaki, New Zealand, *in* Jolley, S.J., et al., eds., Structurally Complex Reservoirs: Geological Society, London, Special Publication 292, p. 235–258, https://doi.org/10.1144/SP292.14.

Çiftçi, N.B., Giger, S.B., and Clennell, M.B., 2013, Three-dimensional structure of experimentally produced clay smears: Implications for fault seal analysis: American Association of Petroleum Geologists Bulletin, v. 97, p. 733–757, https://doi.org/10.1306/10161211192.

Daigle, H., and Dugan, B., 2011, Permeability anisotropy and fabric development: A mechanistic explanation: Water Resources Research, v. 47, W12517, https://doi.org/10.1029/2011WR011110.

Dewhurst, D.N., Brown, K.M., Clennell, M.B., and Westbrook, G.K., 1996, A comparison of the fabric and permeability anisotropy of consolidated and sheared silty clay: Engineering Geology, v. 42, p. 253–267, https://doi.org/10.1016/0013-7952(95)00089-5.

Egholm, D.L., Clausen, O.R., Sandiford, M., Kristensen, M., and Korstgård, J.A., 2008, The mechanics of clay smearing along faults: Geology, v. 36, p. 787–790, https://doi.org/10.1130/G24975A.1.

Færseth, R.B., 2006, Shale smear along large faults: Continuity of smear and the fault seal capacity: Journal of the Geological Society, v. 163, p. 741–751, https://doi.org/10.1144/0016-76492005-162.

Grant, N.T., 2020, Stochastic modelling of fault gouge zones: Implications for fault seal analysis, *in* Ogilvie, S.R., et al., eds., Integrated Fault Seal Analysis: Geological Society, London, Special Publication 496, p. 163–197, https://doi.org/10.1144/SP496-2018-135.

International Energy Agency Greenhouse Gas R&D Programme (IEAGHG), 2016, Fault Permeability, 2016/13: Cheltenham, UK, IEAGHG, 160 p., http://documents.ieaghg.org/index.php/s/iqN7FwwEnOdADXr/download (accessed August 2021).

Jolley, S.J., Dijk, H., Lamens, J., Fisher, Q.J., Manzocchi, T., Eikmans, H., and Huang, Y., 2007, Faulting and fault sealing in production simulation models: Brent Province, northern North Sea: Petroleum Geoscience, v. 13, p. 321–340, https://doi.org/10.1144/1354-079306-733.

Kettermann, M., Thronberens, S., Juarez, O., Urai, J.L., Ziegler, M., Asmus, S., and Krüger, U., 2016, Mechanisms of clay smear formation in unconsolidated sediments—Insights from 3-D observations of excavated normal faults: Solid Earth, v. 7, p. 789–815, https://doi.org/10.5194/se-7-789-2016.

Kettermann, M., Urai, J.L., and Vrolijk, P.J., 2017, Evolution of structure and permeability of normal faults with clay smear: Insights from water-saturated sandbox models and numerical simulations: Journal of Geophysical Research: Solid Earth, v. 122, p. 1697–1725, https://doi.org/10.1002/2016JB013341.

Lehner, F., and Pilaar, W., 1997, The emplacement of clay smears in synsedimentary normal faults: Inferences from field observations near Frechen, Germany, *in* Møller-Pedersen, P., and Koestler, A., eds., Hydrocarbon Seals, Importance for Exploration and Production: Norwegian Petroleum Society Special Publication 7, p. 39–50, https://doi.org/10.1016/S0928-8937(97)80005-7.

Lie, K.-A., 2019, An Introduction to Reservoir Simulation Using MATLAB/GNU Octave: User Guide for the MATLAB Reservoir Simulation Toolbox (MRST): Cambridge, Massachusetts, Cambridge University Press, 678 p., https://doi.org/10.1017/9781108591416.

Lindsay, N., Murphy, F., Walsh, J.J., Watterson, J., Flint, S., and Bryant, I., 1993, Outcrop studies of shale smears on fault surfaces, *in* Flint, S., and Bryant, I., eds., The Geological Modelling of Hydrocarbon Reservoirs and Outcrop Analogues: International Association of Sedimentology Special Publication 15, p. 113–123.

Lu, J., Carr, D.L., Treviño, R.H., Rhatigan, J.-L.T., and Fifariz, R., 2017, Evaluation of Lower Miocene confining units for CO_2 storage, offshore Texas state waters, northern Gulf of Mexico, USA, *in* Treviño, R.H., and Meckel, T.A., eds., Geological CO_2 Sequestration Atlas of Miocene Strata, Offshore Texas State Waters, No. RI0283: Austin, Texas, University of Texas at Austin, Bureau of Economic Geology, p. 14–25, https://doi.org/10.23867/RI0283D.

Lunn, R.J., Shipton, Z.K., and Bright, A.M., 2008, How can we improve estimates of bulk fault zone hydraulic properties?, *in* Wibberley, C.A.J., et al., eds., The Internal Structure of Fault Zones: Implications for Mechanical and Fluid-Flow Properties: Geological Society, London, Special Publication 299, p. 231–237, https://doi.org/10.1144/SP299.14.

Manzocchi, T., Walsh, J.J., Nell, P., and Yielding, G., 1999, Fault transmissibility multipliers for flow simulation models: Petroleum Geoscience, v. 5, p. 53–63, https://doi.org/10.1144/petgeo.5.1.53.

Myers, R.D., Allgood, A., Hjellbakk, A., Vrolijk, P., and Briedis, N., 2007, Testing fault transmissibility predictions in a structurally dominated reservoir: Ringhorne Field, Norway, *in* Jolley, S.J., et al., eds., Structurally Complex Reservoirs: Geological Society, London, Special Publication 292, p. 271–294, https://doi.org/10.1144/SP292.16.

Myers, R.D., Vrolijk, P.J., Kiven, C.W., and Tsenn, M., 2014, Method for predicting fluid flow: U.S. Patent 8,793,110, https://patents.google.com/patent/US8793110B2 (accessed October 2022).

Noorsalehi-Garakani, S., Kleine Vennekate, G.J., Vrolijk, P., and Urai, J.L., 2013, Clay-smear continuity and normal fault zone geometry—First results from excavated sandbox models: Journal of Structural Geology, v. 57, p. 58–80, https://doi.org/10.1016/j.jsg.2013.09.008.

Rawling, G.C., Goodwin, L.B., and Wilson, J.L., 2001, Internal architecture, permeability structure, and hydrologic significance of contrasting fault-zone types: Geology, v. 29, p. 43–46, https://doi.org/10.1130/0091-7613(2001)029<0043:IAPSAH>2.0.CO;2.

Ringrose, P.S., and Meckel, T.A., 2019, Maturing global CO_2 storage resources on offshore continental margins to achieve 2DS emissions reductions: Scientific Reports, v. 9, 17944, https://doi.org/10.1038/s41598-019-54363-z.

Snippe, J., Kampman, N., Bisdom, K., Tambach, T., March, R., Maier, C., Phillips, T., Inskip, N.F., Doster, F., and Busch, A., 2022, Modelling of long-term along-fault flow of CO_2 from a natural reservoir: International Journal of Greenhouse Gas Control, v. 118, https://doi.org/10.1016/j.ijggc.2022.103666.

Sosio de Rosa, S., Shipton, Z.K., Lunn, R.J., Kremer, Y., and Murray, T., 2018, Along-strike fault core thickness variations of a fault in poorly lithified sediments, Miri (Malaysia): Journal of Structural Geology, v. 116, p. 189–206, https://doi.org/10.1016/j.jsg.2018.08.012.

Sperrevik, S., Gillespie, P.A., Fisher, Q.J., Halvorsen, T., and Knipe, R.J., 2002, Empirical estimation of fault rock properties, *in* Koestler, A.G., and Hunsdale, R., eds., Hydrocarbon Seal Quantification: Norwegian Petroleum Society Special Publication 11, p. 109–125, https://doi.org/10.1016/S0928-8937(02)80010-8.

Treviño, R.H., and Meckel, T.A., 2017, Geological CO_2 Sequestration Atlas of Miocene Strata, Offshore Texas State Waters, No. RI0283253: Austin, Texas, University of Texas at Austin, Bureau of Economic Geology, 74 p., https://doi.org/10.23867/RI0283D.

Tveranger, J., Braathen, A., Skar, T., and Skauge, A., 2005, Centre for Integrated Petroleum Research: Research activities with emphasis on fluid flow in fault zones: Norsk Geologisk Tidsskrift, v. 85, p. 63–71, https://njg.geologi.no/vol-81-90/details/17/363-363.

Vrolijk, P.J., Urai, J.L., and Kettermann, M., 2016, Clay smear: Review of mechanisms and applications: Journal of Structural Geology, v. 86, p. 95–152, https://doi.org/10.1016/j.jsg.2015.09.006.

Weber, K., Mandl, G., Pilaar, W., Lehner, B., and Precious, R., 1978, The role of faults in hydrocarbon migration and trapping in Nigerian growth fault structures, *in* Proceedings of the 10th Offshore Technology Conference: Houston, Texas, p. 2643–2653, https://doi.org/10.4043/3356-MS.

Yielding, G., 2012, Using probabilistic shale smear modelling to relate SGR predictions of column height to fault-zone heterogeneity: Petroleum Geoscience, v. 18, p. 33–42, https://doi.org/10.1144/1354-079311-013.

Yielding, G., Freeman, B., and Needham, D.T., 1997, Quantitative fault seal prediction: American Association of Petroleum Geologists Bulletin, v. 81, p. 897–917, https://doi.org/10.1306/522B498D-1727-11D7-8645000102C1865D.

Zheng, X., and Espinoza, D.N., 2021, Multiphase CO_2-brine transport properties of synthetic fault gouge: Marine and Petroleum Geology, v. 129, https://doi.org/10.1016/j.marpetgeo.2021.105054.

Printed in USA